CHARACTERISTICS OF IMPULSIVE NOISE IN ELECTRICITY SUBSTATIONS

Qingshan Shan[1], Shahzad Bhatti[1], Ian A Glover[1], Robert Atkinson[2], Iliana E Portugues[3], Philip J Moore[3] and Richard Rutherford[4]

[1]Centre for Excellence in Signal and Image Processing
[2]Centre for Intelligent Dynamic Communications, 3Institute for Energy & Environment
Department of Electronic & Electrical Engineering, University of Strathclyde, 204 George Street, Glasgow G1 1XW
[4]Scottish Power – Energy, Networks & Telecommunications,1 Atlantic Quay, Glasgow G2 8SP
phone: + (44) 1415482663, fax: + (44) 1415522487, email: qingshan.shan@eee.strath.ac.uk, website: www.strath.ac.uk

ABSTRACT

Measurements of noise in an electricity substation are reported. The measurements are made in four contiguous frequency bands covering the range 100 MHz to 6 GHz. The range includes those bands relevant to modern wireless LAN and wireless PAN technologies such as IEEE 802.11a/b/g and IEEE802.15.1/4). Impulsive events are extracted from the measured data and a statistical analysis these events is presented.

1. INTRODUCTION

Impulsive noise has the potential to degrade the performance and reliability of wireless communications systems [1]. Such noise, which is especially prevalent in high-voltage electricity substations, has discouraged electricity utility companies from deploying wireless technologies for operational purposes. If the rise-time of the noise pulses is sufficiently short the frequency spectrum will extend into the gigahertz region [2]. This paper reports the characterisation of impulsive noise from a 400/275/132 kV substation with special attention to noise energy in those microwave frequency bands not previously reported but relevant to new, short-range, technologies (in particular IEEE 802.11a/b/g, Bluetooth, ZigBee). A model of impulsive noise specific to electricity substations is needed to assess the risk associated with the operational deployment of wireless communication technologies for monitoring and control functions in the electricity supply industry (ESI).

An impulsive noise process, common in substations and which has received much recent attention, occurs due to partial discharge (PD). This is the result of partial breakdown in a dielectric resulting in an impulsive (and random) component of current. The emphasis, here, however, is on the aggregate impulsive noise background irrespective of its physical origin.

Whilst impulsive noise is strong close to its source it decays rapidly with distance [3]. To characterise it properly, therefore, may require its extraction from a mixture of other unwanted signal and noise processes including coherent interference (e.g. broadcast and other radio communications and radar signals). This makes practical site-characterisation difficult since PD sources may be significant distances from buildings where measurement equipment can be protected against environmental effects (in particular humidity and the ingress of water). An effective method of extracting PD from a background of higher-power noise and interference processes is therefore desirable.

Several methods of extracting impulsive noise from other noise processes have been investigated [4] and the wavelet transformation has been identified as being particularly useful [5]. Wavelet packet transformation (WPT) represents a generalisation of the wavelet transform [6].

An application of WPT for online PD detection in 11 kV cables has been reported [7]. The parent wavelet used was symlet-6 (Figure 1) with 8-level decomposition. This method was shown to have a recovery probability of 60% for 1 ns impulses buried in white noise with a standard deviation 1.25 times greater than the peak pulse voltage. Whilst this work suggests that the performance of the WPT depends on wavelet selection as well as on SNR (the optimum wavelet being related to the duration of the impulses of interest), PD noise originating from cables has been successfully recovered from a noisy background (comprising both random and coherent processes) without any priori knowledge of the PD characteristics.

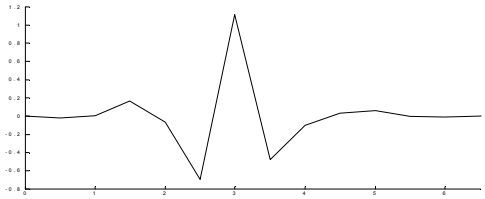

Figure 1 – Symlet-6 wavelet.

WPT has been used in conjunction with neural networks to separate corona from PD in a gas-insulated substation [8]. In this application 5-level wavelet packet decomposition (WPD) using the symlet-8 wavelet was used. Energy, kurtosis and skew values were computed for each node in the WPD tree. Using large between-class and small within-class scatter criteria, feature data were selected from these values. With the feature data as inputs, a three-layer feed-forward neural network with a back-propagation learning rule was used to classify PD, corona and mixed signal (PD plus corona) events. The method successfully removed corona from a mixed signal data set.

© EURASIP, 2009

2. MEASUREMNTS

The noise measurement campaign was undertaken at Strathaven 400/275/132 kV air-insulated electricity substation in central Scotland, Figure 2. The substation is owned and operated by Scottish Power Ltd., a UK electricity utility. A detection system was deployed in the control room of the substation.

Figure 2 – Strathaven substation 400 kV compound.

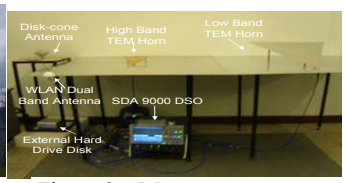

Figure 3 – Measurement system deployed in substation.

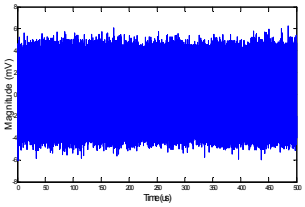

Figure 4 – Raw measurement.

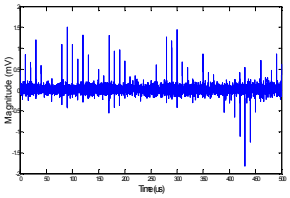

Figure 5 – De-noised impulses.

The measurement system [9], shown in Figure 3, comprises a low-band TEM horn (LBH, 716 MHz - 1.98 GHz), a high-band TEM horn (HBH, 1.905 – 5.1 GHz), a disk-cone antenna (0 - 800 MHz), a dual-band (2.4/5.2 GHz) WLAN antenna, a four-channel digital storage oscilloscope (DSO) (bandwidth 0 - 6 GHz) and an external hard disk drive (HDD). The antennas are connected directly to the DSO. The signals are simultaneously sampled at 20 GS/s. Each data record comprises 50 M samples corresponding to a 2.5 ms time-series. The records are saved to the HDD via a USB interface. It takes approximately 15 minutes for the system to complete one measurement/save cycle. An example of a raw (unprocessed) measurement is shown in Figure 4.

3. PROCESSING

Two stages of processing are employed to extract impulsive events. The first separates impulsive from non-impulsive 'noise' processes. We refer to this as 'de-noising'. The second identifies the important features (e.g. rate, amplitude, duration, rising time, pulse incident times within 2.5 ms time window and pulse spacing) of the de-noised impulses.

3.1 De-noising impulses

Wavelet packet transformation is central to the extraction of impulses from the Strathaven measurement records [10]. The signal processing involves four steps:

- Decomposition of both approximation and detail. Wavelet packet decomposition of the signal is computed up to level 12 using the symlet-6 wavelet
- Computation of best tree. The optimal wavelet packet tree with Stein's unbiased risk estimate (SURE) entropy function is computed
- Wavelet-packet coefficient thresholding. Hard thresholding is applied to the coefficients of each packet (except for the approximation)
- Reconstruction. The required signal is reconstructed based on the original approximation coefficients at each level and the modified detail coefficients.

An example of de-noised impulses, from the original measurement shown in Figure 4, is given in Figure 5.

3.2 Extraction of impulse features

The volume of data measured is large (12 TB) and the volume processed to date is 250 GB. The feature extraction algorithm is therefore required to be as simple as possible to keep processing costs manageable. A basic feature extraction algorithm developed in this study comprises the following seven steps:

- Calculation of threshold value. Threshold value, T, is the lesser of T_1 and T_2 given by:

$$T_1 = \frac{1}{k}\max\left|X_j - \frac{\sum_{i=1}^{N} X_i}{N}\right| \quad (1)$$

and

$$T_2 = \frac{l}{N}\sum_{j=1}^{N}\left|X_j - \frac{\sum_{i=1}^{N} X_i}{N}\right| \quad (2)$$

where X is the de-noised data time series, N is the number of samples and $k = 4$ and $l = 6$. The values of k and l are experimental results chosen for extracting relatively accurate number of impulses from de-noised results.

- Formation of time index clusters. Transition data, M_j, is defined by:

$$M_j = X_j - \frac{\sum_{i=1}^{N} X_i}{N} \quad (3)$$

A cluster is identified as a set of contiguous data points satisfying $|M_j| > T$. The values of X_j corresponding to one time index cluster represent one impulse,

- Extraction of impulse amplitude. Impulse amplitude is the maximum value found from X_j within a time index cluster,
- Extraction of occurrence time of impulse. The occurrence time of an impulse is the time index (measured from the start of the data segment) corresponding to the maximum value of the time cluster,
- Calculation of impulse duration. The impulse duration is the difference of time indices corresponding to locations on either side of the maximum value that are $1/\sqrt{2}$ of the maximum value,
- Calculation of impulse rise-time. The rise-time of the pulse is the difference of time indexes corresponding to 10% and 90% of the pulse's maximum amplitude,
- Calculation of inter-arrival time between impulses. The inter-arrival time is the difference of occurrence times of 2 successive impulses.

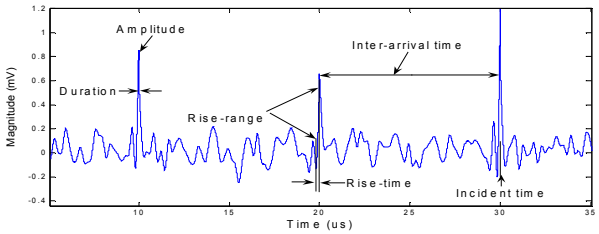

Figure 6 – Illustration of impulse features.

The impulse features are illustrated in Figure 6, which is a time-dilated segment Figure 5.

4. RESULTS

The probability distributions (PDFs) of (a) impulse rate, (b) impulse amplitude, (c) impulse duration, (d) impulse rise-time, (e) impulse occurrence time and (f) impulse spacing have been calculated for the feature data extracted from 197 instances of data measured via the disk-cone, LBH and HBH antennas respectively. The distributions along with the best fit analytical curves are shown in Figures 7 – 9.

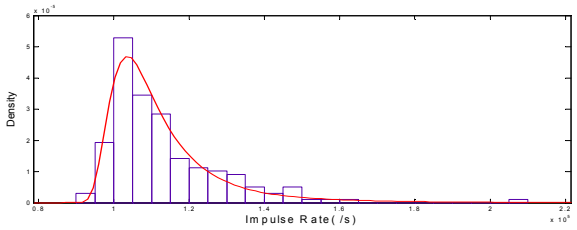

Figure 7(a) – PDF of (disk-cone) mean impulse rate (/s).

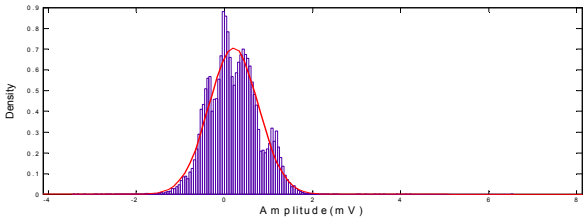

Figure 7(b) – PDF of (disk-cone) impulse amplitude.

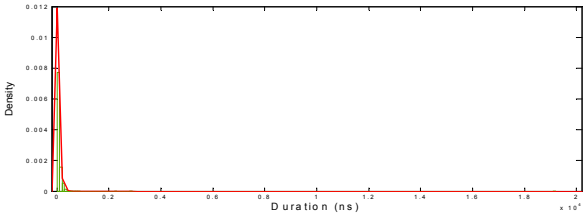

Figure 7(c) – PDF of (disk-cone) impulse duration.

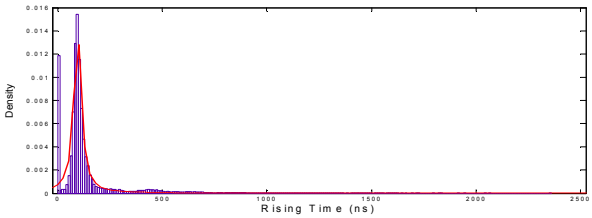

Figure 7(d) – PDF of (disk-cone) impulse rise-time.

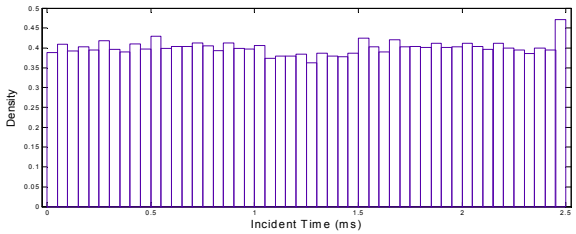

Figure 7(e) – PDF of (disk-cone) impulse occurrence time within 2.5 ms time series segment.

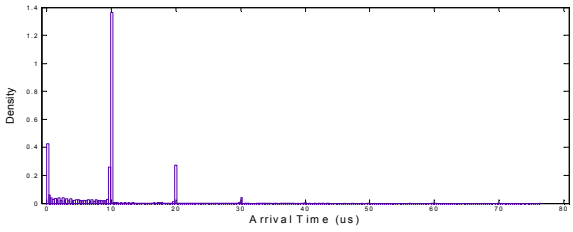

Figure 7(f) – PDF of (disk-cone) inter-pulses arrival time.

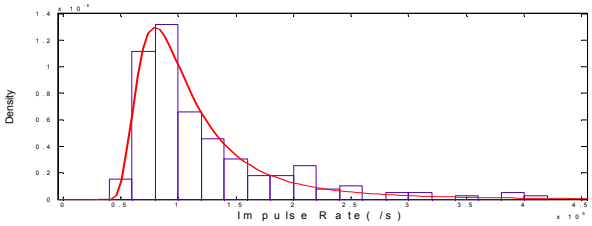

Figure 8(a) – PDF of (LBH) PDF of mean impulse rate (/s).

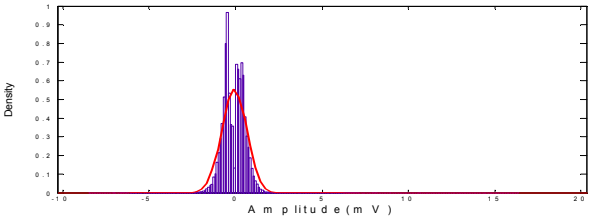

Figure 8(b) – PDF of (LBH) amplitude of impulses for.

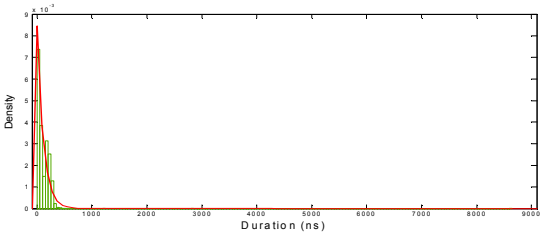

Figure 8(c) – PDF of (LBH) the duration of impulses.

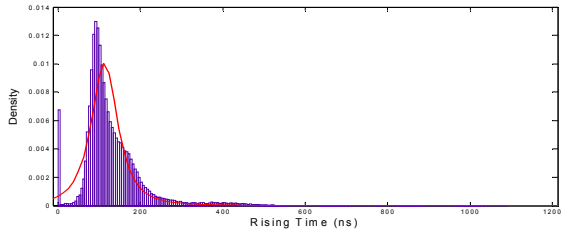

Figure 8(d) – PDF of (LBH) impulse rise time.

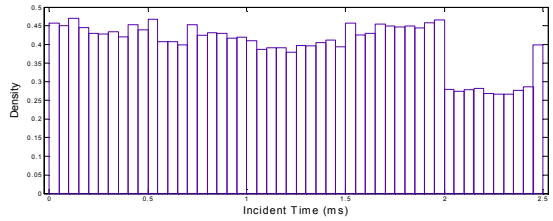

Figure 8(e)– PDF of (LBH) incident time of impulses within 2.5 ms.

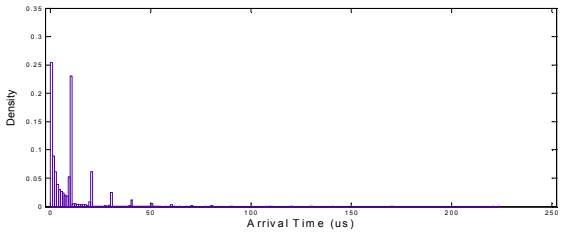

Figure 8(f) – PDF of (LBH) inter-pulses arrival time.

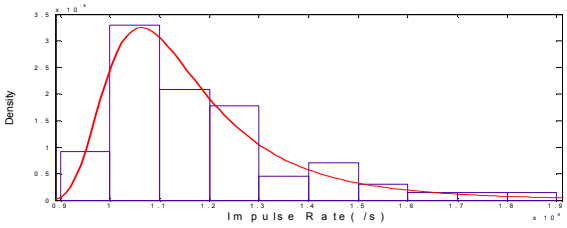

Figure 9(a) – PDF of (HBH) mean impulse rate (/s).

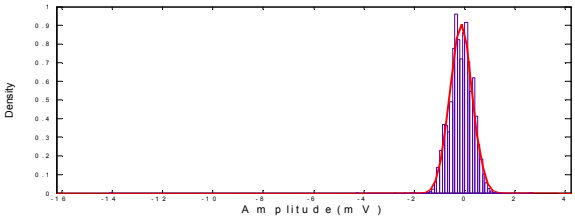

Figure 9(b) – PDF of (HBH) amplitude of impulses.

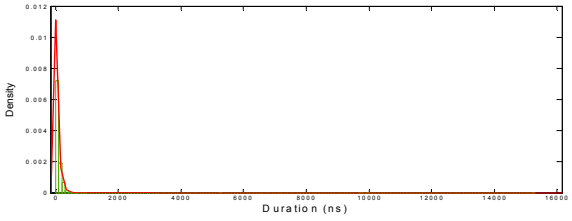

Figure 9(c) – PDF of (HBH) duration of impulses.

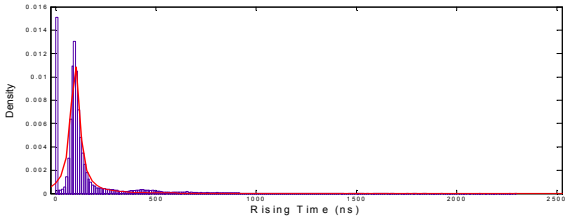

Figure 9(d) – PDF of (HBH) impulse rise-time.

Table 1 shows the best-fit parameters of the distributions for each set of measured data. The distributions selected for each data set have been determined subjectively from the following distribution types: Beta, Binomial, Birnbaum-Saunders, Exponential, Extreme Value, Gamma, Generalized Extreme Value, Generalized Pareto, Inverse Gaussian, Log-Logistic, Logistic, Lognormal, Nakagami, Negative Binomial, Normal, Poisson, Rayleigh, Rician, t Location-Scale and Weibull.

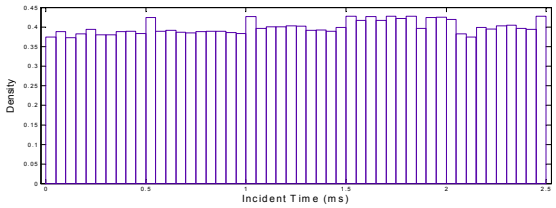

Figure 9(e)–PDF of (HBH) incident time of impulses within 2.5 ms.

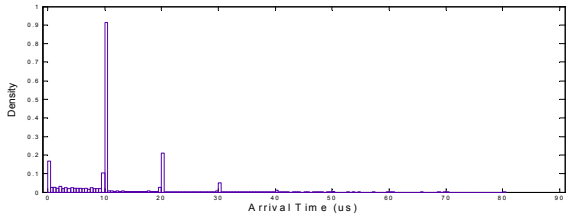

Figure 9(f) – PDF of (HBH) inter-pulses arrival time.

4. DISCUSSION

Impulse rate (r) follows a generalised extreme value distribution, i.e.:

$$y = f(r \mid \nu, l, s) = \left(\frac{1}{s}\right) \exp\left(-\left(1+\nu\frac{(r-l)}{s}\right)^{-\frac{1}{\nu}}\right)\left(1+\nu\frac{(r-l)}{s}\right)^{-1-\frac{1}{\nu}} \qquad (4)$$

where l, s and ν are location, scale and shape parameters, respectively. This distribution is often used to model the smallest or largest values in a large set of independent, identically distributed, random variables. The mean value (around 10^5 pulse/s, see Table 1) is similar for all antennas. The variance, however, appears to be sensitively dependent on antenna type; factors of 10 and 1000 relating, respectively, the variance for HBH and LBH antennas to the disk-cone antenna. Location, scale and shape parameters are similar for all three antennas.

Impulse amplitude is Gaussianly distributed with a mean value close to zero for all antennas. (This is a consequence of the similarity between statistics of positive and negative impulses.) The variance is also similar for all antenna types.

Impulse duration is exponentially distributed with a similar mean for all antennas of around 90 ns.

Impulse rise-time (τ) is t location-scale distributed, i.e.:

$$y = f(\tau \mid \nu, l, s) = \frac{\Gamma\left(\frac{\nu+1}{2}\right)}{s\sqrt{\nu\pi}\,\Gamma\left(\frac{\nu}{2}\right)}\left[\nu + \frac{(\tau-l)}{s}\right]^{-\left(\frac{\nu+1}{2}\right)} \qquad (5)$$

The location parameter in (5) is of the order of 100 ns, the scale parameter is around 30 ns and the shape parameter is close to unity. The differences between antenna types appear to be relatively small.

The time of occurrence distribution (measured from the start of each 2.5 ms time-series data-segment) is approximately uniform.

Table 1 – The parameters of fitted distributions

Process	Antenna	Distribution	Parameter	
Impulse rate	Diskcone	Generalized Extreme Value	μ	1.13×10^{5} s^{-1}
			σ^2	3.48×10^{7} s^{-1}
			l	1.05×10^{5} s^{-1}
			s	8.12×10^{3} s^{-1}
			ν	2.76×10^{-1}
	LBH	Generalized Extreme Value	μ	1.24×10^{5} s^{-1}
			σ^2	1.04×10^{10} s^{-1}
			l	8.90×10^{4} s^{-1}
			s	3.02×10^{4} s^{-1}
			ν	3.77×10^{-1}
	HBH	Generalized Extreme Value	μ	1.18×10^{5} s^{-1}
			σ^2	5.34×10^{8} s^{-1}
			l	1.08×10^{5} s^{-1}
			s	1.16×10^{4} s^{-1}
			ν	2.34×10^{-1}
Impulse amplitude	Diskcone	Gaussian (Normal)	μ	2.11×10^{-1} mV
			σ^2	3.19×10^{-1} mV
	LBH	Gaussian (Normal)	μ	-7.57×10^{-2} mV
			σ^2	5.19×10^{-1} mV
	HBH	Gaussian (Normal)	μ	-1.48×10^{-1} mV
			σ^2	1.94×10^{-1} mV
Impulse duration	Diskcone	Exponential	μ	7.77×10^{1} ns
			σ^2	6.04×10^{3} ns
	LBH	Exponential	μ	1.15×10^{2} ns
			σ^2	1.33×10^{4} ns
	HBH	Exponential	μ	8.50×10^{1} ns
			σ^2	7.22×10^{3} ns
Impulse rise time	Diskcone	t location-scale	l	9.57×10^{1} ns
			s	2.08×10^{1} ns
			ν	8.69×10^{-1}
	LBH	t location-scale	l	1.13×10^{2} ns
			s	3.51×10^{1} ns
			ν	1.95×10^{0}
	HBH	t location-scale	l	9.67×10^{1} ns
			s	2.68×10^{1} ns
			ν	9.05×10^{-1}

μ - mean value; σ^2 - variance; l - location; s - scale; ν – shape

The inter-pulse spacing distribution has a quasi-discrete character with approximately constant spacing between pdf peaks. This suggests a single dominant source of impulsive noise with an underlying (approximate) periodicity, and appears to preclude partial discharge as the dominant process. The physical origin of this process is, as yet, obscure and is currently under investigation.

5. CONCLUSION

Measurements of the electromagnetic noise environment in an electricity substation have been reported using microwave antennas covering a contiguous band of frequencies from 100 MHz to 6 GHz. Algorithms for extracting impulsive events have been describe and used to construct a database of impulsive noise. A statistical analysis of impulse rate, amplitude, duration, rise-time, occurrence time and spacing has been presented.

A model of impulsive noise based on the statistical and spectral characteristics measured for the assessment of risk associated with wireless equipment deployment in substations is under construction.

ACKNOWLEDGMENT

The UK Engineering & Physical Sciences Research Council (EPSRC) is gratefully acknowledged for financial support of this project under Grant EP/D049687/1.

REFERENCES

[1] M.G. Sanchez, I Cuinas, and A. V. Alejos, "Interference and impairments in radio communication systems due to industrial shot noise,"IEEE International Symposium on Industrial Electronics ISIE 2007, PP1849-1854.

[2] M. D. Judd, O. Farish, J. S. Pearson, and B. F. Hampton, "Dielectric windows for UHF partial discharge detection," IEEE Transactions on Dielectrics and Electrical Insulation, vol. 8, pp. 953-958, 2001.

[3] M. Hikita, H. Yamashita, T. Hoshino, T. Kato, N. Hayakawa, T. Ueda, and H. Okubo, "Electromagnetic noise spectrum caused by partial discharge in air at high voltage substations," Power Delivery, IEEE Transactions on, vol. 13, pp. 434-439, 1998.

[4] S. Sriram, S. Nitin, K. M. M. Prabhu, and M. J. Bastiaans, "Signal denoising techniques for partial discharge measurements," Dielectrics and Electrical Insulation, IEEE Transactions on [see also Electrical Insulation, IEEE Transactions on], vol. 12, pp. 1182-1191, 2005.

[5] L. Satish and B. Nazneen, "Wavelet-based denoising of partial discharge signals buried in excessive noise and interference," Dielectrics and Electrical Insulation, IEEE Transactions on [see also Electrical Insulation, IEEE Transactions on], vol. 10, pp. 354-367, 2003.

[6] S. Mallat, A wavelet tour of signal processing, 2nd ed. London: Academic Press, 1999.

[7] A. Kyprianou, P. L. Lewin, V. Efthimiou, A. Stavrou, and G. E. Georghiou, "Wavelet packet denoising for online partial discharge detection in cables and its application to experimental field results," Measurement Science and Technology, vol. 17, pp. 2367-2379, 2006.

[8] C. S. Chang, J. Jin, C. Chang, T. Hoshino, M. Hanai, and N. Kobayashi, "Separation of corona using wavelet packet transform and neural network for detection of partial discharge in gas-insulated substations," Power Delivery, IEEE Transactions on, vol. 20, pp. 1363-1369, 2005.

[9] Q Shan, I A Glover, R Rutherford, S Bhatti, R Atkinson, I E Portugues, P J Moore, "Detection of UWB impulsive noise in 400 kV electricity substation," CIRED 20th International Conference on Electricity Distribution, Prague, Czech Republic (in press).

[10] Q Shan, S Bhatti, I A Glover, R Atkinson, P J Moore, I E Portugues, R Rutherford, "Extraction of impulsive noise from measurements in a 400 kV electricity substation," The 2009 International Energy and Environment Conference, Cambridge, UK.